Asian Journal of Nanoscience and Materials 2 (2019) 286-300

Asian Journal of Nanoscience and Materials

Journal homepage: www.ajnanomat.com

Original Research Article

Preparation of different manganese oxide structures *via* controlling the concentration and the type of the alkaline media

Samer Said, Mary Raid*, Sara Mikhail

Egyptian Petroleum Research Institute, Nasr City, Egypt

ARTICLE INFORMATION

Received: 1 October 2018
Received in revised: 21 October 2018
Accepted: 2 November 2018
Available online: 2 February 2019

DOI: 10.26655/AJNANOMAT.2019.2.3.4

KEYWORDS

Transvermillion
Olanzapine
Piper betel
Films
Biopolymer

ABSTRACT

Birnessite and manganite materials were prepared using a simple precipitation process in an alkaline medium. Potassium hydroxide and tetraethyl ammonium hydroxide (TEAH) used as the precipitating agents. Different techniques such as XRD, DSC, TGA, FT-IR, TEM and N_2 adsorption analyses were employed to characterize the prepared samples. The results revealed that the formed phase in the prepared sample is dependent on the concentration of the precipitating agent. In addition, the XRD results showed the formation of various phases through controlling the concentration of the precipitating agent. Pure phase of birnessite produced in the high alkaline medium, and manganite (γ-MnOOH) at relatively low alkalinity. The samples prepared by using TEAH were well crystalline compared with the analogue one prepared by KOH. The obtained results elaborated the role of TEAH in directing the order of the particles during the preparation step.

Graphical Abstract

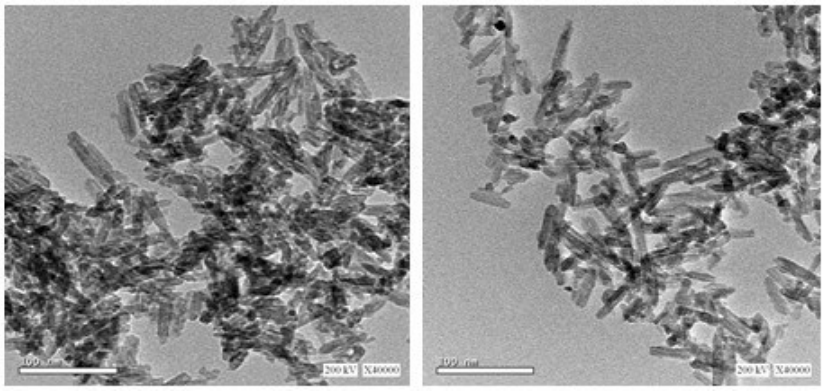

Corresponding author, email: maryriad2006@yahoo.com (M. Raid).
Tel.: 01227930864.

Introduction

Among the metal oxides, manganese dioxide is one of the most attractive inorganic materials because of its stability towards high temperature, acidic or basic conditions of different reactions. These reactions include the catalytic ozonation of oxalic acid [1], trans-esterification of soybean [2], oxygen evolution, and oxygen reduction [3]. MnO_2 has several crystallographic forms because the basic octahedral units "MnO_6" are linked in different ways [4].

The layered manganese oxides are classical type of inorganic host layer as birnessite [5], lithiophorite [6], cryptomelane [7, 8], romanechite, hollandite [9], and todorokite [10]. Natural δ-MnO_2 (birnessite) is a highly disordered and occurred in a finely dispersed state, commonly mixed with other phases such as phyllosilicates and Fe oxy-hydroxides.

Birnessite has gained a great deal of attention as an electrode material for super capacitors because of its thin sheet-like lamellar structure, which is similar to the hydrated ruthenium oxide [11]. In addition, it can be ordered to facilitate the cations intercalation/de-intercalation process [12]. Because of the structural defects, and large specific surface area; birnessite plays an important role in the heavy metals [13], and other pollutants removal [14]. It can be used as a highly sensitive and selective hydrogen gas sensor [15], catalysis [16], ion exchange, and energy storage [17]. Several methods were developed to prepare the birnessite-type MnO_2 structures, including hydrothermal synthesis [18], micro-emulsion route [19], sol gel [20], electro-deposition [21], and microwave-assisted route [22].

This work provides an interesting cheap and non-toxic approach to prepare the manganese oxides with diverse controllable structure, texture, and phase purity in an alkaline medium. The controlled reactions allow the large-scale and the cost-effective synthesis of birnessite and manganite materials.

Experimental

The materials used in this study were of analytical grade (purity: 99.99%), purchased from Sigma-Aldrich company, and used without further purification.

Preparation of birnessite material

To prepare the birnessite sample, 500 mL of 0.2 mol $MnSO_4$ solution, 1.5 mol KOH, and 10% vol/vol of H_2O_2 were mixed in a conical flask, under air bubbling at a flow rate of 150 r/min for 5h. After that, the obtained precipitate (birnessite) centrifugally separated, washed several times with distilled water (until pH of the filtrate reaches 7), and air-dried.

Preparation of manganite material

To prepare manganite sample, 500 mL of 0.2 mol $MnSO_4$ solution, 0.15 mol KOH, and 10% vol/vol of H_2O_2 were mixed in a conical flask, under air bubbling at a flow rate of 150 r/min for 5 h. The obtained precipitate (manganite, γ-MnOOH) centrifugally separated, washed several times with distilled water (until pH of the filtrate reaches 7), and air-dried. The formed phases of either birnessite, and or manganese oxides were controlled by different factors as; the concentration & type of the precipitating agent, the presence of an oxidant (H_2O_2), and the effect of calcination temperature.

Structural phase changes

X-ray diffraction pattern (XRD) was carried out on a Shimadzu XD-1 diffracto-meter using Cu $K_\alpha$radiation (λ=0.1542 nm) at a beam voltage

of 40 kV and 40 mA beam current. The Joint Committee on Powder Diffraction Society (JCPDS) database used to index the peaks of XRD. Average crystallite size was calculated using Sherrer's equation from X-ray line broadening using the most intense peak at 2θ = 12.3° (birnessite), and 35.6° (manganite). These peaks are well resolved and showed no interferences. Determination of the lattice constants of the samples were made by refinement of the XRD data and match software using the Rietveld full profile method, Chi square value =2.7 [23].

Fourier transform infrared (FT-IR) was investigated using a spectrometer Perkin-Elmer -Spectrum^{-1} (4000–400 cm^{-1}) at a resolution of 4 cm^{-1}. Before measurement, the samples were grounded, and dispersed in KBr to compress into pellets.

Differential scanning calorimetry-thermo-gravimetric (DSC-TGA) was performed on SDTQ-600 (TA-USA) thermo balance instrument. 10 mg of sample was heated up to 1000 °C, with a heating rate of 10 °C . min^{-1} under air-flow at a rate of 100 mL min^{-1}.

N_2-adsorption measurements were performed at -196 °C in a Micromeritics 2000 ASAP analyzer to determine the specific surface area and pore size distribution.

High-resolution transmission electron microscopy (HRTEM) images of the samples were recorded on a JEOL JEM-2100F microscope operating at voltage of 200 kV. The samples were prepared by dispersing in ethanol and sonicated for 20 min. The suspension was dropped on a carbon coated copper grid for TEM observations.

Results and Discussion

Factors affecting the preparation of different phases of manganese oxide

Effect of the oxidant concentration

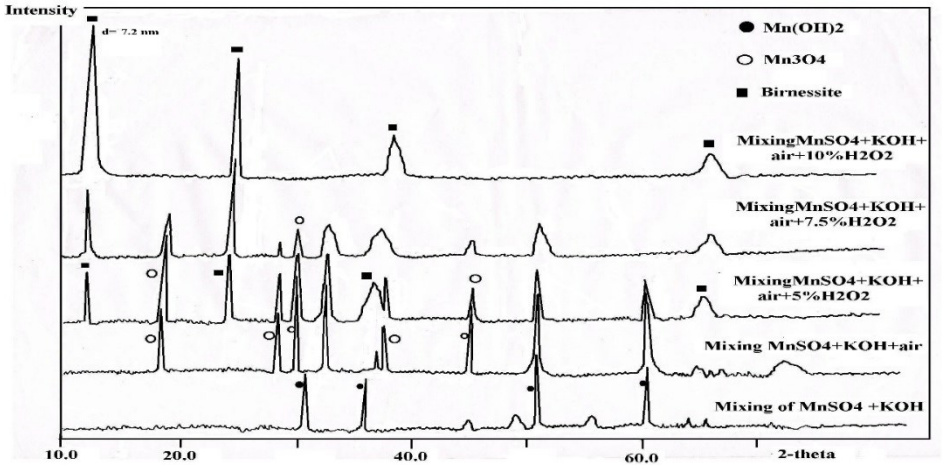

Figure 1. Effect of the presence of oxidant on the formed manganese oxide samples

X-ray diffraction pattern (Figure 1) displayed the sample obtained on mixing manganese sulphate and potassium hydroxide (1.5 mol). Data in figure reflect the appearance of sharp lines at 2θ= 30.5, 35.4, 50.07, and 60.0° in which were identified as crystalline Mn $(OH)_2$-(JCPDS-01-73-1604). Initially, on drop-wise addition of KOH, the pH in the vicinity of the drop becomes alkaline leading to the formation of a white colored $Mn(OH)_2$. Upon stirring, the pH became acidic and the precipitate re-dissolved. Gradually, as the pH

becoming more alkaline crystalline $Mn(OH)_2$ was precipitating in place of re-dissolving.

Under air bubbling, which is favored as an oxidant, the diffracto-gram (Figure 1) detects lines at 2θ=18.2, 29.4, 30.7, 32.4, 36, 38.2°, 44.9, 50.9°, and 60°. These lines are matched with the tetragonal husmannite, (JCPDS-24-0734, with lattice constants a=b=0.5765 nm, and c = 0.9442 nm). This means that, $Mn(OH)_2$ is substantially converted to brown colored husmannite (Mn_3O_4) under air bubbling. Otherwise, as the airflow is not enough to facilitate the birnessite formation, different concentrations of H_2O_2 added as co-oxidant.

Upon the addition of 5% (vol/vol) H_2O_2, the XRD pattern (Figure 1) reveals the detection of two distinct major peaks at 2θ=12.3° and 24.7° and two broad ones at 2θ=37.1° and 65.7°. These peaks are assigned to the planes of MnO_2 with a birnessite structure (JCPDS-1456-43, hexagonal symmetry, a=b=0.279 and c=0.725 nm) [24]. Besides, other diffraction lines that characterize the presence of husmannite was observed.

Birnessite has a lamellar structure consisting of one Mn-(III)O_6 octahedral chain inserted between two Mn(IV)O_6 octahedral chains. The interlayer distance of MnO_6 octahedral layers is 0.73 nm. The broadening of the peaks revealed that the formed birnessite product has a small crystallite size with a poor crystalline structure.

With the progressive increasing in concentration of H_2O_2 from 5 to 7.5%, the husmannite diffraction lines became weak. The pure birnessite phase formed after adding 10% (vol/vol) H_2O_2.

Effect of the concentration of the precipitating agent

Inorganic precipitating agent (potassium hydroxide, KOH)

Concentration of the alkaline solution (KOH) is a factor to determine the type of manganese oxide phase. The precipitation process for manganese species was carried out using KOH concentrations: 0.05, 0.15, 0.5, 1.0, and 1.5 mol (the concentration of H_2O_2 is 10% vol/vol). At a relatively low KOH concentration (0.05 mol), the diffraction pattern (Figure 2) reveals the appearance of diffraction lines at 2θ=21.8°, 36.9°, 41°, and 55.8°. These lines reflect the formation of γ-MnO_2 phase (JCPDS -14-0644).

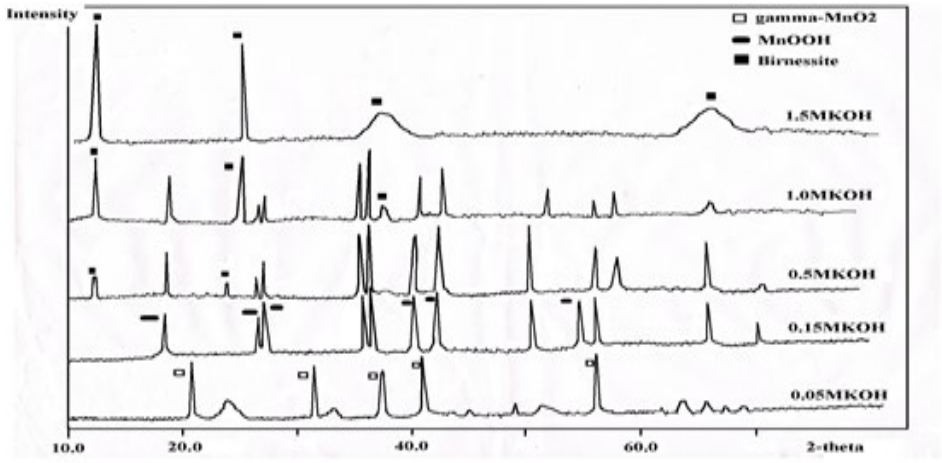

Figure 2. Effect of Concentration of KOH on the Formed Manganese Oxide Samples

γ-MnO_2 is favored to form at nearly neutral medium as postulated by *De Wolff* [25] who prepared MnO_2 by redox reaction of Mn^{+7} at pH=8.

With gradual increasing in the concentration of KOH to 0.15 mol, sharp peaks are observed at 2θ=18, 26.22, 34.01, 35.63, 39.62, 51.31, and 65.53° (Figure 2). These peaks characterized the formation of manganite (γ- MnOOH, JCPDS-41-1379, a=5.29, b = 5.263 and c=5.304 Å). Thus, by increasing the concentration of the KOH (0.15 mol.), MnO_2 collapsed, dissolved, re-crystallized, and formed γ-MnOOH with a high surface-energy. The progress increase in KOH concentration to 0.5 mol. (Figure 2), clarified a slight increase in the intensity of diffraction lines characterizing the MnOOH phase. In accordance, the birnessite diffraction lines were intimately detected. By further increasing the concentration of KOH to 1.0 mol, the formation of birnessite was increased in parallel with the gradual decrease of MnOOH formation. Pure birnessite phase is detected on using 1.5 mol KOH. As clarified, the use of an oxidant under air bubbling may compensate the need of sufficient quantity of the alkaline agent to form birnessite phase. Therefore, the most-selected KOH concentration is 1 mol. This result conflicts with *Gai* et al., [26] data who studied the preparation of birnessite via the oxidation of Mn^{+2} in the presence of an oxidant under alkaline condition (the concentration of alkaline agent reached ~5.5 mol).

Organic precipitating agent (tetraethyl ammonium hydroxide, TEAH)

The effect of type of the precipitating agent (TEAH, 0.05-1.0 mol concentration range) on the structure of the formed phases was studied. The pattern (Figure 3) reveals the disappearance of γ-MnO_2 phase on using 0.05 mol TEAH, which was due to the presence of an electrostatic interaction. The negatively charged surface of MnO_2 could easily adsorb the positively charged TEAH ions, either on the surface and or entered the tunnel for negative charge compensation. Accordingly, some strains are created in the MnO_2 tunnel structure that is easily destroyed and then re-crystallized to form MnOOH phase (2θ=18, 26.22, 34.01, 35.63, 39.62, 51.31, and 65.53°).

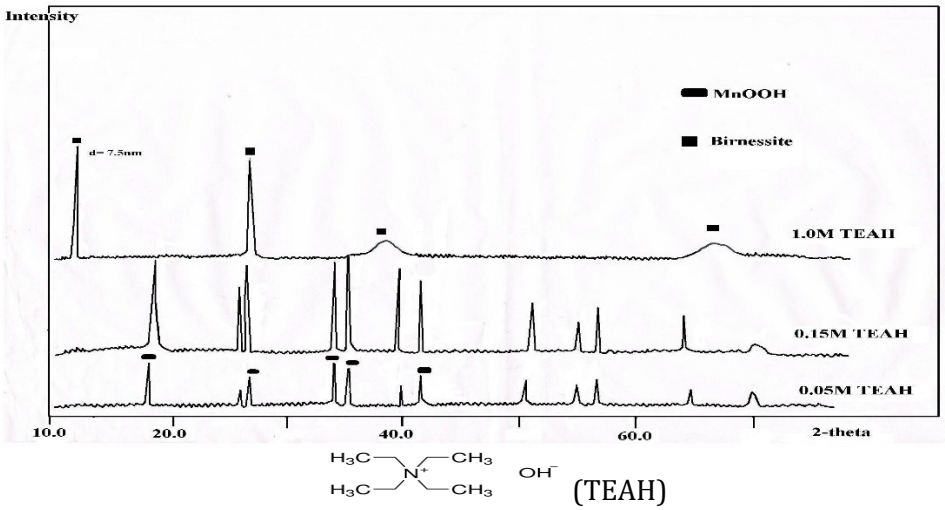

Figure 3. Effect of concentration of TEAH on the formed manganese oxide samples

On using 0.15 mol. TEAH, sharp diffraction lines with high intensities were detected (Figure 3), correspond to the formation of pure MnOOH phase. This result suggested that the TEAH could induce an electrostatic repulsion forces between particles. The growth rate of the

particles reduced to a point to prevent their agglomeration. Thus, the obtained particles during the initial precipitation step were ordered and well-dispersed ones. On using 1.0 mol TEAH, the pattern (Figure 3) reflects the presence of sharp and broad peaks at 2θ=12.3°, 24.7°, 37.1°, and 65.7°, which are consistent with hexagonal ordering of birnessite phase. It is obvious that, the interlayer spacing (0.75 nm, 2θ=11.8°), is larger than that for birnessite (0.72 nm–using KOH) [26]. This result suggests that both of anionic and cationic parts containing TEAH species could be incorporated in-between birnessite layers. These species induce a repulsive hydration and then a high fraction of interlayer space formed and filled with water and proton ions. Besides, the unit cell volume is bigger (103.7 A°) than the analogue (103.0 A°, KOH), resulting in the weakness of Mn–O bond strength. This may provide the sample with a concentration of ion pairs (Mn^{3+} and Mn^{4+}) on the surface.

Effect of calcination temperature

The effect of calcination temperature was studied at 300, 450, and 600 °C to investigate the thermal transformation of the precipitated manganese oxide phases. The X-ray diffraction pattern (Figure 4) for MnOOH-KOH sample calcined at 300 °C, represented diffraction lines at 2θ=29.0, 37.5, 41, 43.5, 56.3, and 59.5°, which indexed to a tetragonal β-MnO_2 phase (JCPDS-24-0735, a=0.4397, c=0.2872 nm).

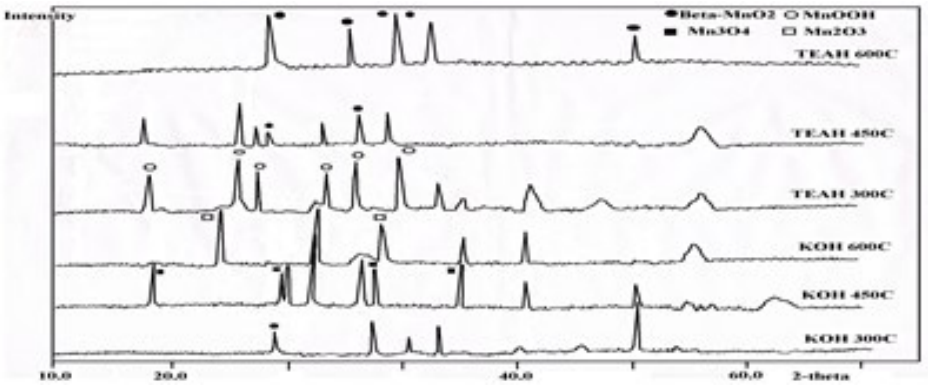

Figure 4. XRD for the MnOOH sample calcined at different temperatures

With further increase in calcination temperature to 450 °C, diffraction lines are detected at 2θ=18.2, 29.4, 30.7, 32.4, 36, 38.2, 44.9, 50.9, and 60° (Figure 4) and can be indexed to Mn_3O_4 phase. With the increase in the temperature to 600 °C, diffraction lines (Figure 4) are detected at 2θ=24, 32.5, 39, 45, 50, 55, and 65.5°, which corresponded to the formation of a cubic bixbyte Mn_2O_3 phase (JCPDS-41-1442, a=0.941 nm).

From point of view, the obtained results in this study agreed with the data postulated by *Atique Ullah* et al., [27].

They informed that Mn_3O_4 transformed to Mn_5O_8 phase at 500 °C, and completely transformed to cubic Mn_2O_3 at 700 °C, (Equations 1-3):

$4MnOOH+O_2$ (250-300 °C) → 4 β-MnO_2+2 H_2O(gas) (1)

$6MnOOH + 5/2O_2$ (350-400 °C) → $2Mn_3O_4$+3 H_2O (gas) (2)

$Mn_3O_4+2/5O_2$ (500 °C) →$3/5Mn_5O_8$, Mn_5O_8 is subsequently converted to Mn_2O_3 at 700 °C (3)

Meanwhile, *Vro* et al., [28] represent that manganite (γ-MnOOH) transformed to Mn_2O_3 at 350-450 °C. After that, it can be transformed to Mn_3O_4 at 900-1000 °C temperature range, *via*

the reduction reaction of Mn_2O_3 and the oxygen evolution.

On the other hand, the pattern (Figure 4) for MnOOH-TEAH sample, calcined at 300 and 450 °C detects diffraction lines at 2θ=18, 26.22, 34.01, 35.63, 39.62, 51.31, and 65.53°. These diffraction lines are consistent with the γ-MnOOH phase but with low intensities. On increasing the calcination temperature to 600 °C, diffraction lines are detected corresponding to the formation of β-MnO_2 phase. The formation of β-MnO_2 at high temperature suggested that TEAH could increase the stability of the formed γ-MnOOH phase and retarded its transformation up to 600 °C [29].

XRD pattern for the birnessite –KOH sample calcined at 300 °C (Figure 5) detected the presence of Mn_3O_4 phase, which was formed via the decomposition of birnessite at 300 °C. At calcination temperature 450 °C, the pattern (Figure 5) detected lines at 2θ=12.8°, 18.5°, 28.9°, 37.5°, 42°, and 50°, corresponds to the formation of tunnel-structured manganese oxide (cryptomelane, JCPDS-29-1020). On further increase in the calcination temperature to 600 °C, birnessite is de-hydrated; re-structured and pure cryptomelane phase is formed [11].

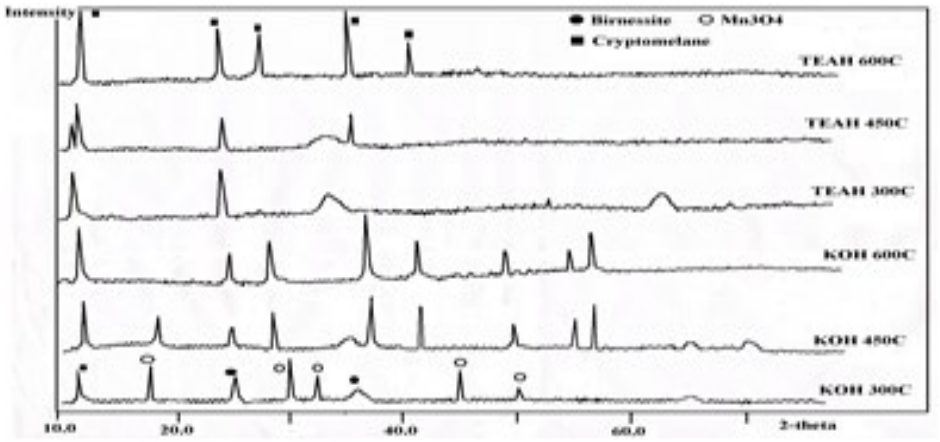

Figure 5. XRD for the birnessite calcined at different temperature

Structural characterization

Average crystallite size

The crystallite size for the prepared materials was calculated using both XRD and TEM**.** The crystallite size for MnOOH -KOH actually decreased from 15.3 to 11.0 nm for the analogue using TEAH. The decrease in crystallite size from 33.5 to 17.0 nm was also observed for birnessite -TEAH, in parallel with the results obtained from TEM (Table 1). Thus, the increase in the electron donating capacity of ethyl-group (TEAH) favored the formation of smaller crystallite size.

Table 1. Crystallite Size for the prepared Samples

Samples	Crystallite Size (nm)	
	XRD	TEM
Birnessite-KOH	33.5	28.7
Birnessite-TEAH	17.0	12.7
MnOOH -KOH	15.3	11.5
MnOOH -TEAH	11.0	6.2

Fourier transform infrared

FT-IR spectrum for MnOOH -KOH sample (Figure 6) displayed bands at 593, 712, and 488 cm^{-1} that characterize Mn–O stretching vibration of γ-MnOOH in tetrahedral and octahedral sites [30]. The broad bands at 2084 and 2672 cm^{-1} correspond to the fundamental O–H stretching bands related to hydrogen bonds, with an O–H· · ·O in the structure of manganite [31]. The bands at 1089, 1120, and1196 cm^{-1} are typical of the γ-OH, δ-2-OH, and δ-1-OH bending modes, respectively. The bands assigned at 1636 and 3413 cm^{-1} are related to the adsorbed water molecules on the particle surfaces. The observed band at 2069 cm^{-1} is attributed to the binary combinations involving the OH vibrations of manganite [32]. FT-IR spectrum for birnessite -KOH sample displays bands in the region between 400 and 800 cm^{-1}, which could be assigned to Mn–O lattice vibration [33]. The bands at 513, 478, and 413 cm^{-1} are in good agreement with the IR characteristic bands of layered manganese oxides. Besides, these bands correspond to Mn-O stretching modes of the octahedral layers in the birnessite structure. While, the bands assigned at 730, 670, 627, and 578 cm^{-1}, are related to the vibration modes (wagging, bending, symmetrical, and asymmetrical stretching) of the octahedral layers of Mn–O bonds in birnessite structure [34].

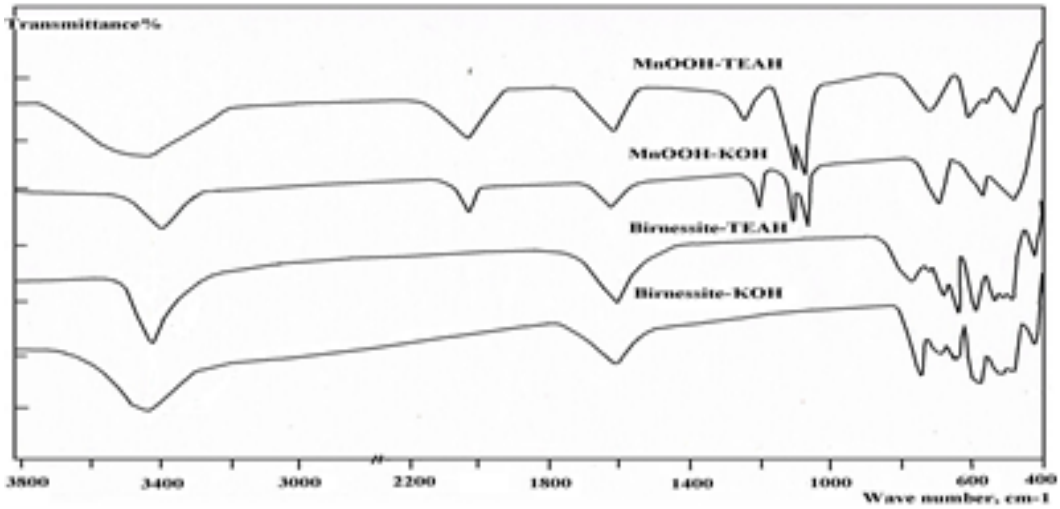

Figure 6. FT-IR for the prepared samples

The stretching band at 1614 cm^{-1} corresponds to the angular deformation of the molecular water. The broad band at ~ 3420 cm^{-1} was an indicative to the stretching and bending vibrations of water molecules or hydroxyl groups in the interlayer.

Changing the precipitating agent to TEAH causes a slight shift in the positions of the characterized Mn–O bands (bending and stretching modes). These changes resulted from the increase in the crystalline order of TEAH-samples, which was in accordance with the XRD results. In addition, the pronounced increase of band intensity at 3433 cm^{-1} is observed more for the prepared TEAH-samples than for KOH ones. Such increase was attributed to the increase of the hydroxyl groups or tunnel water species. Moreover, the two sharp bands at 2850 and 2914 cm^{-1} are assigned to the symmetric and asymmetric stretching modes of the $-CH_2$ group of TEAH. The symmetric and asymmetric vibrations of $(CH_3)_4–N^+$ groups are associated with the band at 1510 cm^{-1}. The band located at

930 cm^{-1} is assigned to the C–N^+ stretching mode of TEAH [35].

Thermal analysis

Differential scanning calorimetry (DSC) and thermo-gravimetric (TG) analyses for the prepared samples are displayed in Figure 7 and 8.

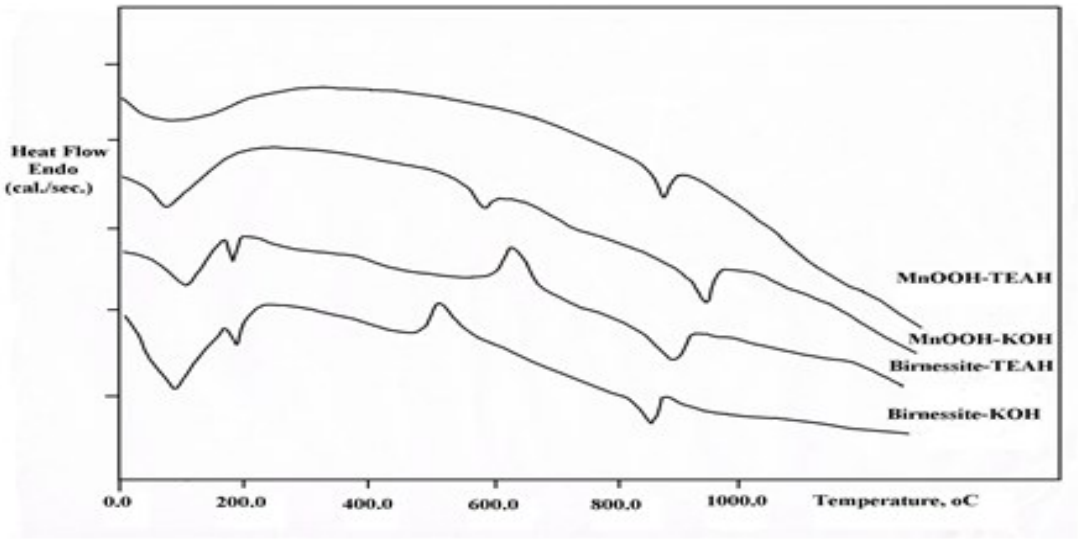

Figure 7. DSC Profiles for the prepared samples

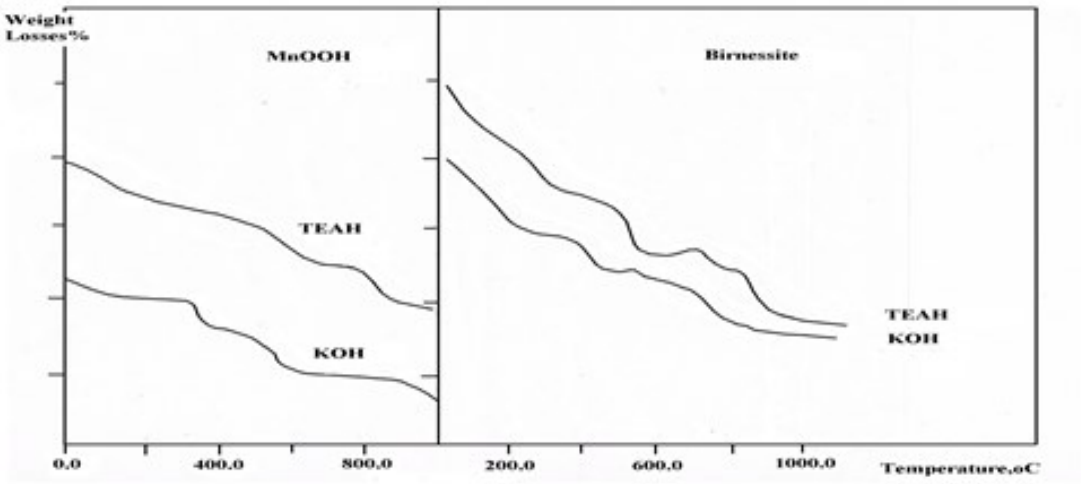

Figure 8. TG Profile for the prepared samples

DSC profile for birnessite -KOH sample (Figure 7) reveals the presence of endothermic peaks at ~80 and 180 °C. These peaks correspond to the removal of the physically adsorbed water and some of the crystallized water from the interlayer of the birnessite, respectively. As evidenced from XRD results at reaction temperature 300 °C, the birnessite structure is unchanged, which reflects its thermal stability. On the other hand, the exothermic peak detected at 500 °C is related to the phase transformation of K-birnessite to cryptomelane that had one-dimensional (2 × 2) tunnel with K^+ in the tunnel site, in agreement

with Rives et al, results [36]. The endothermic peak detected at 820 °C is attributed to the collapse of the cryptomelane structure and its transformation to manganese oxide species [37]. On contrary, the DSC profile for birnessite -TEAH sample ascribes the slow behavior of TEAH on the oxidation process of birnessite. The transformation of the birnessite -TEAH to cryptomelane was decelerated as the exothermic peak is delayed and started to appear at 600 °C, which is consistent with XRD results. The TG profile for birnessite – KOH sample (Figure 8) illustrates four steps with total weight losses of 9.5 wt%. The first weight loss (6.25 wt%, in the 25-210 °C temperature range) resulted from the removal of the adsorbed water. The second one (0.85 wt%, at 210-480 °C) is attributed to the partial reduction of Mn^{4+} to Mn^{3+}, and the released oxygen from the oxide [17]. The third step (at 480-750 °C) shows a slight weight gain (-0.6 wt%), which is ascribed to the phase transformation via the oxidation of Mn^{3+} to Mn^{4+}. The fourth one (2.36 wt%, at 750–840 °C) is related to the structural transformation from MnO_2 to manganese oxide species.

TG profile for birnessite -TEAH sample (Figure 8) behaves similarly as KOH but with higher weight loss values (11.54, 2.46, and 4.24 wt %), which may include the decomposition of TEAH molecules and suggested the hygroscopic nature of this sample. Thus, the total content of physisorbed and structural coordinated water of birnessite -TEAH is more than that of the birnessite -KOH samples. This was because the tetra-ethyl ammonium hydroxide molecules exhibit a stronger affinity to OH anions. DSC profile for MnOOH- KOH sample (Figure 7) reflects the presence of only two obvious endothermic peaks.

As known, the transformation of γ-MnOOH to β-MnO_2 is an isomorphic transformation. Whereas, the hydrogen may be removed from the channels of γ-MnOOH under heating and subsequently β-MnO_2 is formed. Therefore, there is no indication that this transformation can be detected by DSC profile. The observed DSC peaks may be due to the crystal transformation of β-MnO_2 to other manganese oxidation states. DSC profile for the analogue one (TEAH) displays only one endothermic peak at 850 °C, which may be due to the complete transformation of MnOOH to the stable oxide form Mn_2O_3., in agreement with XRD data. The weight loss for MnOOH samples can be categorized into four segments (Figure 8), with total weight losses (12.7 wt%). The first weight loss (0.3 wt%, at 50–170 °C) results from the removal of the physical adsorbed water. The weight loss (2.9 %, at 310–370 °C) is due to the decomposition of γ-MnOOH to β-MnO_2. The subsequent weight losses (~ 6.8 and 2.7 %, at 500-580 °C and 800-900 °C) are due to the crystal transformation of MnO_2 to the other manganese oxidation states.

On the other hand, the TGA profile for MnOOH-TEAH sample displayed three weight loss steps (Figure 8). These steps are due to: the removal of adsorbed water, the subsequent transformation of MnOOH into β-MnO_2, Mn_2O_3 phases and the decomposition of TEAH molecules. The total weight loss (10.8 wt%) is lower than that of KOH, and confirms the stability of the formed material.

Texture characterization

The N_2 adsorption–desorption isotherms and pore size distribution plot of the prepared samples using different precipitating agents are represented in Figure 9.

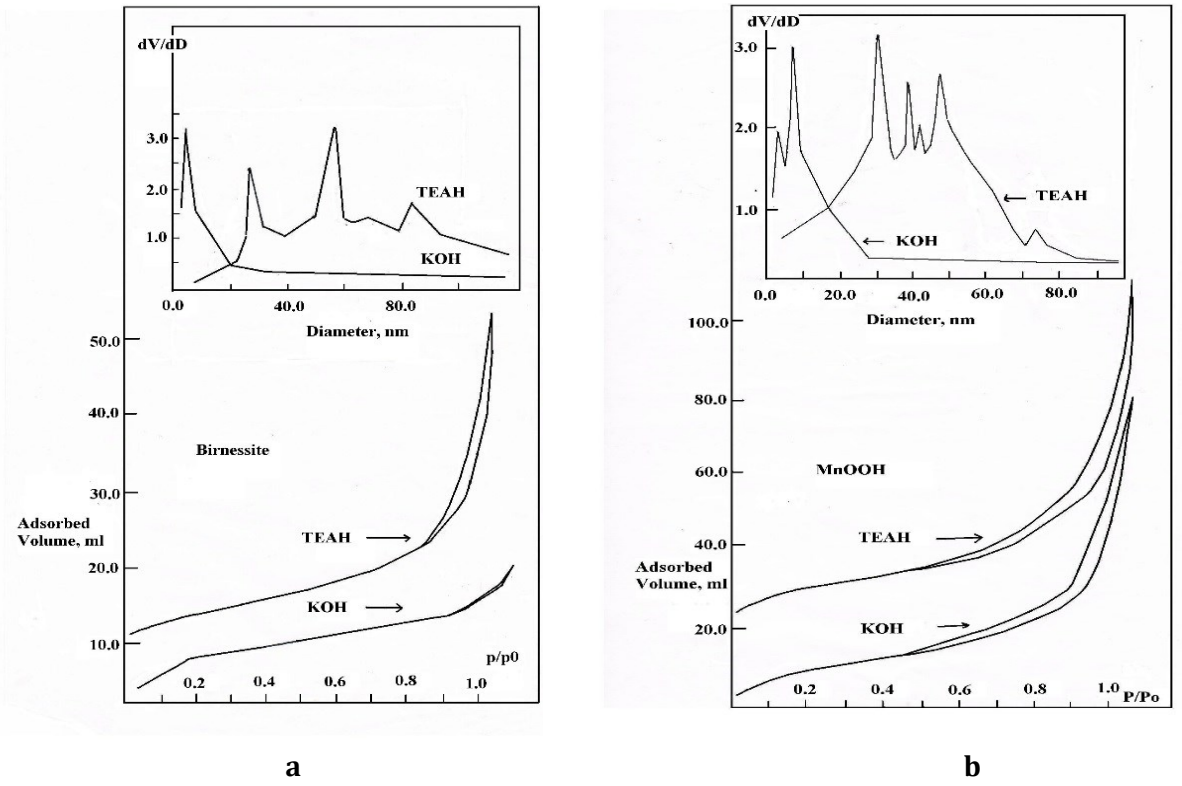

Figure 9. Adsorption-desorption isotherms and pore size distribution for a) Birnessite, b) MnOOH samples

The textural properties including BET surface area, total pore volume, and average pore diameter are tabulated in Table 2.

Table 2. Surface texture parameters for the prepared Samples

Sample	S_{BET} m^2 g^{-1}	V_P, cm^3 g^{-1}	r_H, nm
Birnessite-KOH	16.17	0.039	0.18
Birnessite-TEAH	35.3	0.21	0.37
MnOOH -KOH	21.4	0.32	0.13
MnOOH -TEAH	50.8	0.46	0.29

The isotherm for birnessite- KOH sample configured no clear capillary condensation and hysteresis loop at high p/p^0 indicating its poorly porous nature. In contrast, birnessite -TEAH sample exhibits type II isotherm with H3 hysteresis loop (according to the IUPAC classification). This result suggested the presence of slit-like pores formed by the stacking of sheet-like building. On the other hand, data (Table 2) clarified the low value of BET surface area (16.17 m^2/g) and total pore volume (0.039 cm^3/g), which are visualized for birnessite – KOH sample. Thus, the sample exhibits poor crystalline structure, which would not contribute much to either surface area and/or pore volume. Meanwhile, the relatively higher surface area (35.3 m^2 g^{-1}) and pore volume (0.21 cm^3 g^{-1}) of birnessite –TEAH sample are attributed to the order of birnessite sheets. The prepared MnOOH samples (KOH

and TEAH) exhibit type IV isotherm with H3 hysteresis loop that indicated the meso-porous nature of the prepared samples. The abrupt nitrogen uptake and a narrow hysteresis loop at P/P^0 range of 0.6-0.95 for MnOOH-TEAH suggested the presence of an interstitial space between the particles. The surface area of MnOOH -TEAH (50.8 $m^2 g^{-1}$) is higher than that of the analogue one (KOH, 21.4 $m^2 g^{-1}$). The aggregates degeneration induced by the TEAH may be the reason for such increase in surface area.

Pore size distribution

The pore size distribution curves derived from the desorption branch for birnessite and MnOOH samples are graphically illustrated in Figure 9. The low crystalline nature of birnessite -KOH sample leads to its poor pore structure and eventually to a narrow pore size distribution around 4.9 nm. On the other hand, birnessite -TEAH sample exhibits multi-pore size distributions (20-100 nm), in parallel with the increase in: S_{BET}, V_p, and the amount of adsorbed gas. This behavior may be related to the intercalation of TEAH in between birnessite sheets, causes merging of some narrow pores and creation of other new meso-pores.

MnOOH -KOH sample exhibits bi-modal pore size distribution centered at 2.2 and 6.3 nm, which reveals its meso-porosity.

For MnOOH-TEAH sample numerous pores are generated in the range 40-80 nm, which suggested the creation of meso- and wide meso-pores. TEAH molecules may greatly orient the growth of particles that lead to the generation of pores via the spaces between the particles as indicating from the increase in pore volume.

High resolution transmission electron microscopy

The morphology of the prepared samples of birnessite and manganite with either KOH and or TEAH were investigated by HR-TEM. The images (Figure 10) show that the prepared samples consisted of fine needle-like nano-rods with regular shape. The average diameters are 28.7 and 11.5 nm for birnessite and manganite (KOH), respectively, in agreement with *Xi* et al. data [38]. Meanwhile, the TEM images for the samples prepared using TEAH show dispersed, more uniform nano-rods with an increase in the length and a noticeable decrease in the average diameter (12.7, 6.2 nm for birnessite and manganite, respectively).

KOH TEAH

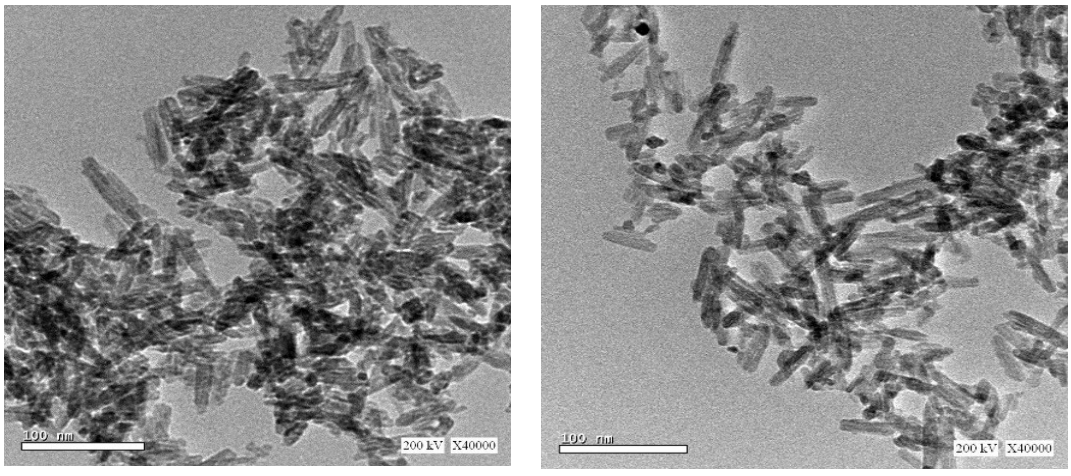

a

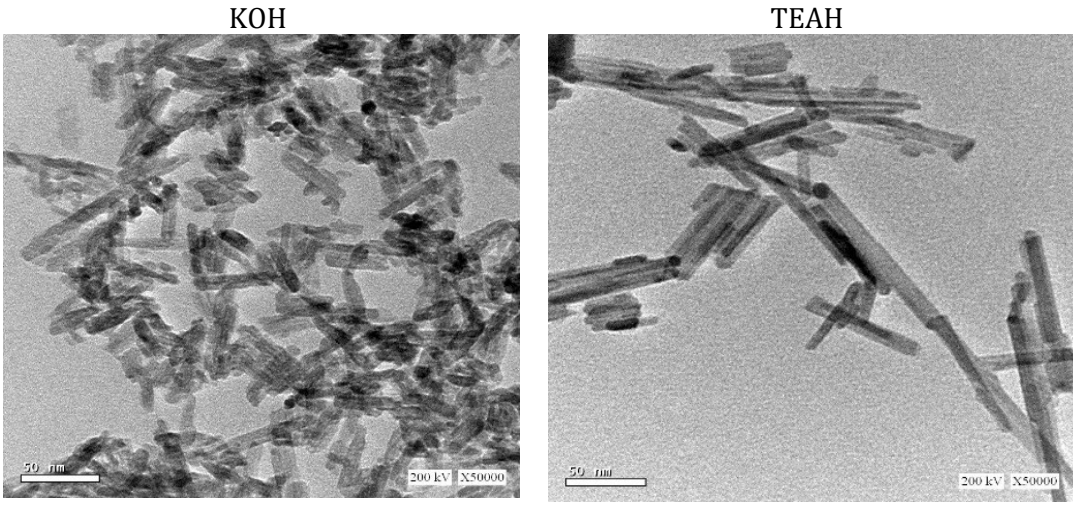

Figure 10. TEM images for a) Birnessite, b) MnOOH samples

Reaction steps for producing either manganite and/or birnessite

Manganite was formed via the precipitation of Mn^{2+} in a basic medium (at pH=8-9) in presence of air and H_2O_2 as oxidant reagents. Firstly, the hydrolysis of Mn^{2+} gives rise to $Mn(OH)_2$. Part of the precipitate may undergo the oxidation in air, according to the following equations (4-6):

$$Mn^{+2} + 2OH^- = Mn(OH)_2 \quad (4)$$

$$4Mn(OH)_2 + H_2O_2 = 4MnOOH + 2H_2O \quad (5)$$

The over all chemical reactions involved:

$$MnSO_4 + H_2O_2 + 2NaOH = MnOOH + 2H_2O + Na_2SO_4 + 1/2H_2 \quad (6)$$

At pH=13, with the participation of dissolved oxygen, a lower oxidation state of manganese Mn^{+2} is fast oxidized and restructured to form the birnessite structure ($Mn^{+3,+4}$). Birnessite under alkaline conditions consist of vacancy free Mn octahedral layers and many negative charges that are associated with the substitution of Mn^{3+} for Mn^{4+}. Layer–layer stabilization in birnessite occurs by means of a strong association of K^+ with the excessive negative charge in the layers

Besides, there is a hydrogen bonding between layer O atoms and interlayer H_2O molecules. When the potassiumions in the birnessite are replaced by TEAH, H-birnessite phase is formed. The existence of K^+ or H^+ ions (besides ethyl group) controlled the size of the tunnel and played a decisive role for transformation of birnessite to cryptomelane under thermal treatment [39]. The cryptomelane was formed via the intercalation (pillaring) of the octahedral MnO_6 into the K-birnessite sheets. The pillars eventually coalesce to form a vertical set of octahedral sheets of cryptomelane structure, which yields a 2 × 2 tunnel structure. The large size of ethyl group helps to prevent the birnessite layers from collapsing during the thermal process. The process of preparation of cryptomelane with $MnSO_4$ and KOH occurred as follows (Equations 7, and 8):

$$Mn^{2+} + 2OH^- \rightarrow Mn(OH)_2 + O_2 \rightarrow \text{hausmannite } (Mn^{2+}, Mn^{3+}) + H_2O_2 \rightarrow MnOOH\ (Mn^{3+}) \quad (7)$$

$$MnOOH + OH^- + H_2O_2 \rightarrow \text{K-birnessite } (Mn^{3+} > Mn^{4+}) + \text{Heat} \rightarrow \text{cryptomelane } (Mn^{3+} < Mn^{4+}) \quad (8)$$

Conclusions

From the previous work it can be concluded that:
Manganite and Birnessite have potential application in many fields as: catalysis, ion exchange, energy storage, removal of the heavy metals and can be used as a highly sensitive and selective hydrogen gas sensor.

- Birnessite and manganite are prepared by simple, inexpensive and effective oxidation of $MnSO_4$ solution with H_2O_2 in an alkaline medium, either KOH and/or TEAH. Manganite is formed at low pH value in presence of KOH as an alkaline medium while birnessite is formed at high pH value.
- Manganite and birnessite prepared by using TEAH, exhibit high surface area and meso-porosity, in comparing with the analogue prepared by using KOH. Controlling the concentration and type of alkaline medium tuned easily: the crystalline nature, specific surface area, and pore size distribution of the formed manganese oxide phases.
- The precipitating agent TEAH plays an important role in directing the crystallization of reactants to form birnessite and manganite with high surface area, at low temperature.

Disclosure statement

No potential conflict of interest was reported by the author.

References

[1]. Yu, J., Ph. Savage. *Industrial Engineering Chemical Resresearch*, 2000, **39**:4014
[2]. Singh A., Fernando S. Ch*emical Engineering Technology*, 2007, **30**:1716
[3]. Meng Y., Song W., Huang H., Ren Z., Chen S.Y., Suib S. *Journal of Amrican Chemical Society*, 2014, **136**:11452
[4]. Ahsanulhaq Q., Kim S.H., Hahn Y.B. *Journal of Alloys and Compounds*, 2009, **484**:17
[5]. Manceau A., Lanson M., Takahashi Y., *American Mineralogy*, 2014, **99**:2068
[6]. Yang D.S., Wang M.K. *Clays-Clay Mineral*, 2003, **51**:96
[7]. Said S., Riad M., Helmy M., Mikhail S., Khali L. *Journal of Nanostructure Chemistry*, 2016, **6**:171
[8]. Said S., Riad M., Helmy M., Mikhail S., Khali L. *Chemical Material Research*, 2014, **6**:27
[9]. Kitchaev D., Dacek S., Sun W., Ceder G. *Journal of American Chemical Society*, 2017, **139**:2672
[10]. Atkins A.L., Shaw S., Peacock C.L. *Geochimistry Cosmochimistry Acta,* 2014 **144**:109
[11]. Regmi R., Tackett R., Lawes G. *Journal of Management Material*, 2009, **321**:2296
[12]. Athouel L., Arcidiacono P., Ramirez-Castro C., Crosnier O., Hamel C., Dandeville Y., Guillemet P., Scudeller Y., Guay D., Belanger D., et al. *Electrochimical Acta,* 2012, **86**:268
[13]. Villalobos M., Escobar-Quiroz I.N., Salazar-Camacho C. *Geochimstry. Cosmochimistry. Acta,* 2014, **125**:564
[14]. Liu G., Chen L., Yu J., Feng N. *Applied Catalysis A: General*, 2018, **568**:157
[15]. Zhang G., Liu Y., Guo F., Hu Y., Liu X.Z., Qian Y. *Solid State Communcation*, 2005, **134**:523
[16]. Saad L., Sobhi Z., Mikhail S. *Egyptian Journal of Petroleum*, 2002, **11**:67
[17]. Tiana X., Yang L., Qing X., Yu K., Wang X., *Sensor Actua. B*., 2015, **207**:34
[18]. Misnon I.I., Abd Aziz R., Zain N.K., Vidhyadharan M. B., Krishnan S.G., Jose R., *Material Research Bulletin*, 2014, **57**:221
[19]. Huang M., Zhang Y.X., Li F., Zhang L.L., Ruoff R.S., Wen Z.Y., Liu Q. *Science Rep*., 2014, **4**:3878
[20]. Yan D., Zhang H., Li S., Zhu G., Wang Z., Xu H., Yu A. *Journal of Alloys and Compdounds*, 2014, **607**:245

[21]. Ghaly M., El-Dars F., Hegazy M., Abdel Rahman R. *Chemical Engineering Journal*, 2016, **284**:1373
[22]. Nakayama M., Nishiyama M., Shamoto M., Tanimoto T., Tomono K., Inoue R. *Journal Electrochemical Society,* 2012*,* **159**:1176
[23]. Dinnebier E., Billinge J. Po*wder Diffraction Theory and Practice The Royal Society of Chemistry*, 2008; p 1-583
[24]. Lefkowitz J., Elzing E. *Chemical Geology*, 2017, **466**:524
[25]. De Wolff P.M. *Acta Crystallography*, 1959, **12**:341
[26]. Gai J., Liu J., Suib S. *Chemical Material*, 2002, **14**:2071
[27]. Atique Ullah A.K.M., Fazle Kibria A.K.M., Akter M., Khan M.N.I., Maksud M.A., Jahan R.A., Firoz S.H. *Journal of Saudi Chemical Society*, 2017, **21**:830
[28]. Vro D., Brsn L., Posr J. *Amircan Mineralogy*, 1989, **74**:177
[29]. Zhang W., Yang Z., Liu Y., Tang S., Han X., Chen M. *Journal of Crystal Growoth*, 2004, **263**:394
[30]. Liu G., Liao S., Zhu D., Hua Y., Zhou W. *Chemical Engineering Journal*, 2012, **213**:286
[31]. Zhang W., Yang Z., Liu Y. *Journal of Crystal Growoth*, 2004, **263**:394
[32]. Sharma P., Whittingham M. *Material Letter*, 2001, **48**:319
[33]. Kang L., Zhang M., Liu Z.H., Ooi K. *Spectrochimica Acta*. *A*., 2007, **67**:864
[34]. Potter R., Rossman G. *Amrican Minerology*, 1979, **64**:1199
[35]. Kohler T., Armbrustor T., Libowitzky E. *Journal of Solid State Chemistry*, 1997, **133**:486
[36]. Rives V., Prieto O., Del Arco M. *Thermochima Acta*., 2003, **401**:95
[37]. Zhang Y., Qin Z., Wang G., Zhu H. Dong M., Li S., Wu Z., Li Z., Wu Z., Zhang J. *Applied Catalysis Environmental B.*, 2013, **129**:172
[38]. Xi G., Peng Y., Zhu Y., Xu L., Zhang W., Yu W., Qian Y. *Material Research Bulletin*, 2004, **39**:1641
[39]. Li Y., Wei D., Du Y. *Chemosphere*, 2015, **119**:282

How to cite this manuscript: Samer Said, Mary Raid*, Sara Mikhail. Preparation of different manganese oxide structures *via* controlling the concentration and the type of the alkaline media. *Asian Journal of Nanoscience and Materials*, 2019, 2(3), 286-300. DOI: 10.26655/AJNANOMAT.2019.2.3.4